**Advanced Steel Construction** – Vol. 17 No. 3 (2021) 221–230
**DOI:**10.18057/IJASC.2021.17.3.1


# HYSTERETIC PERFORMANCE OF WEAK-AXIS CONNECTION WITH I-SHAPED PLATES IN STEEL FRAME

Ying-Lu Xu [1, 2, 3, *] and Ji-Ping Hao [1, 2, 3]

[1] *School of Civil Engineering, Xi'an University of Architecture & Technology, Xi'an, 710055, China*
[2] *Key Lab of Structural Engineering and Earthquake Resistance, Ministry of Education（XAUAT）, Xi'an, 710055, China*
[3] *Shaanxi Key Lab of Structure and Earthquake Resistance（XAUAT）, Xi'an, 710055, China*
** (Corresponding author: E-mail: 564319073@qq.com)*

**ABSTRACT**

This paper elucidates numerically the behavior of weak-axis moment connections proposed by welding I-shaped plates in the H-section column to increase connection strength and ductility in steel frame. After validating the numerical methods through comparing the results of numerical analysis and experiments, the effectiveness of the proposed weak-axis connection were examined through comparing to the traditional weak-axis connection. The proposed weak-axis connection could move the highest stresses away from the start-stop points of a weld, and thus preventing the premature brittle fracture of the beam flange welds. The plastic hinge formed away from the beam-column interface, while the local buckling occurred in the weld access holes region in the traditional weak-axis connection. The proposed weak-axis connections can be classified as rigid in a strong-bracing system, and be classified as semi-rigid in weak-supported or unsupported system. And then a series of parametric studies was conducted to better understand the behavior of proposed weak-axis moment connections. The force-displacement relationships, location of the plastic hinge, Mises index (MI), triaxiality index (TI) and rupture index (RI) distributions at the beam flange welds were reported in detail. According to the numerical analysis, the design variables of I-shaped plates and widened flange plate are suggested, along with a design procedure.

**ARTICLE HISTORY**

Received: 6 April 2020
Revised: 14 January 2021
Accepted: 27 January 2021

**KEYWORDS**

Steel frame;
Moment connections;
Weak-axis;
I-shaped plates;
Cyclic performance



## 1. Introduction

Steel moment-resisting frame is considered to have superior ductility, and therefore, it has been widely used in earthquake-prone regions. However, in the 1994 Northridge earthquake and 1995 Kobe earthquake, unexpected and widespread brittle failures were observed, generating concerns regarding the design of connections and construction details of connections, as numerous failures occurred in the welded connections whilst the structure remained in elastic state in the earthquake. Causes for the poor performance of these welded connections of Pre-Northridge were mainly conjectured as the poor workmanship leading to weld defects, and poor detailing connections leading to stress concentrations in welds.

To avoid such unexpected failure, the seismic performance of various moment connections has been extensively investigated since the Northridge earthquake to alleviate the stress concentrations in welds and thus providing reliable ductile performance. Various alternatives to beam-to-column connections by strengthening [1-4] or weakening [5-8] the beam section have been proposed to force the plastic hinge a small distance away from the beam-column interface under cyclic loading. However, most of these studies are related to strong-axis connections [1-8] with less attention being paid to the weak-axis connections. For strong-axis moment connections, the highest stresses always concentrate on the center of the groove weld, while the condition is opposite in the weak-axis moment connections, as the highest stresses always concentrate on the edge of the beam flange groove weld, as shown in Fig. 1, described by Gilton and Uang [9]. As the start-stop points are the most vulnerable parts of a weld, the beam flange weld stresses distribution pattern of weak-axis moment connections in Fig. 1b would make the welds more prone to brittle fracture.

The pertinent study concerning weak-axis moment connections to my knowledge was performed by several researchers, and their studies are as follows. FEMA-355D [10] and Guo [11] pointed out that the traditional weak-axis connections has poor plastic rotation less than 0.03 rad. Gilton and Uang [9] conducted an experimental study for two full-scale weak-axis reduced beam section (RBS) moment connections and also a series of parametric studies. It was found that comparing to specimens without RBS, RBS specimens could significantly reduce the critical strain concentration. While in the experimental study of RBS weak-axis connections conducted by Yu et al. [12], the specimen failed to move out the plastic hinge, and the beam flange welds fractured. Oh et al. [13] conducted an experimental study on weak-axis column-tree connections and results showed that the RBS specimen or the tapered beam flange specimen exerted superior ductile performance and no brittle fracture occurred until 0.05 rad story drift angle. Kim et al. [14], Li et al. [15], and Wang et al. [16] proposed different weak-axis connections mainly connected through bolts and conducted related experimental study to investigate the rotating capacity and bearing capacity.


(a) strong-axis connection (b) weak-axis connection

**Fig. 1** Stress distribution of the beam flange

According to the connection requirements of Code for seismic design of buildings (GB50011-2010), the box section column should be adopted when the column is rigidly connected to beams in two mutually perpendicular directions. While the structure cost will be increased when the box section column is used in the project where the I-section column is sufficient to meet the requirements of force and deformation. It is difficult to avoid the weld damage of beam flange welds in the traditional I-section weak-axis connections. Thus, it is necessary to propose a more suitable connection form for the weak-axis connection of I-section column.

Our team conducted an experimental study about a developed weak-axis connection with box-strengthened panel zone in the past years, including five pure steel beam-column connection specimens and five corresponding composite connection specimens [17]. Test results showed that most specimens failed due to the welding fracture, indicating that the connection details needs to be improved. Based on the previous research, this paper proposed a novel weak-axis connection from, as shown in Fig. 2, which is suitable for the weak-axis connections of I-section column in low and multi-layer steel structure frame. The main feature of the proposed weak-axis moment connections is welding the I-shaped plates (Fig. 2b) in the H-section column. And then the widely adopted in the engineering project flange-welded and web-bolted connection is used as it's easy to fabricate and economical, and the widened flange plate is adopted. In this way, the widened flange plate are able to extend out of the column flanges, and thus this developed weak-axis connection can move the highest stresses away from the start-stop points of a weld, which is obviously different from the traditional weak-axis connections (Fig. 1b). Therefore, the developed weak-axis connection can reduce the fracture potential of the beam flange welds. Meanwhile, the extending parts of I-shaped plates also strengthen the strong-axis connections that the widened flange plates can be arranged between the beam flanges and the I-shaped steel plates in strong-axis connections. And thus, the proposed connection could realize the seismic design criteria of "strong joint and weak component", and move the plastic hinge away from the beam flange welds in both strong-axis and weak-axis connections.

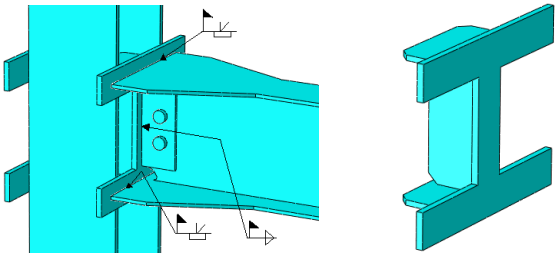

(a) weak-axis connection (b) I-shaped plates

**Fig. 2** Configuration of developed weak-axis connection

The proposed weak-axis moment connections can be constructed by the following procedure:

(1) Cut the steel plates for horizontal stiffeners and vertical stiffeners with the thickness slightly greater than the beam flange and beam web respectively.
(2) Cut two I-shaped steel plates using the anti-lamellar tearing steel plate with the thickness slightly greater than the thickness of the column flange.
(3) Weld two horizontal stiffeners and one vertical stiffener to the I-shaped steel plate, as displayed in Fig. 2b. And the horizontal stiffeners and vertical stiffener aligned with the beam flange and web respectively, as displayed in Fig. 2a.
(4) Weld the I-shaped plates to the column flanges and web, and weld a shear plate to the I-shaped steel plate.
(5) Weld widened flange plates to the end of beam flanges with the thickness same to the beam flange.
(6) Use flange-butt-welded and web-bolted connection method to connect the beam and the I-shaped plate attached to the column.

Based on the general finite element analysis software ABAQUS, a refined tridimensional weak-axis connection model was conducted to replicate the connection specimens in the experimental study depicted in references [11] and [12], parametric studies were undertaken in developing a better understanding of the cyclic performance of the proposed weak-axis connections. This paper is organized as follows. Section 2 introduces the simulation and validation of experimental results. The comparative analysis of the traditional weak-axis connection and the proposed weak-axis connection is conducted in Section 3. Successively, Section 4 presents the parameter analysis of the proposed weak-axis connection. Then, Section 5 discusses the design procedure of the proposed weak-axis connection, and verifies the applicability of the proposed dimensions to other beam and column sections. Finally, conclusions and future developments are drawn in Section 6.

## 2. Simulation and verification of experimental results

Comparing to the experimental study, the numerical modelling has many advantages such as reducing the time and costs, and could explore large numbers of parameters, which has become common in academia. The experimental results of the weak-axis beam-column connection specimen CW-1 in reference [11] and specimen RBS-3 in reference [12] were used as references to verify the effectiveness of the numerical model through comparing the failure mode, and the load versus displacement hysteretic curves.

### *2.1. Modeling techniques and assumptions*

Three-dimensional eight-node solid nonconforming elements (element C3D8I in ABAQUS) were employed for specimens CW-1 and RBS-3 to model the steel profiles. Both material and geometric nonlinearity was considered in the finite element model (FEM). The true stress and plastic strain of the steel profiles was adopted according to the tension coupon tests results described in [11] and [12] respectively. Considering the convergence problem and computational efficiency, different mesh sizes was tried to determine the appropriate meshing methods and conduct the grid sensitivity analysis. The mesh division of the connection and RBS regions was more intensive, and a coarser mesh was adopted elsewhere. Specimens CW-1 and RBS-3 both had one column and one beam, and loading points were at the beam end. Web-bolted flange-welded connection was used for specimens CW-1 and RBS-3. Lateral bracing of the beam was provided for the beam to prevent the lateral deformation of the beam.

### *2.2. 3-D finite element model of CW-1*

For specimen CW-1, the column and beam section was W14×398 and W36×150 respectively, both of A572 Grade 50 steel. 3-D finite element model of CW-1 was display in Fig. 3a. The boundary conditions adopted were the x, y, and z directional displacement restrictions at the top and bottom of the column followed closely those used in the tests. Length of column and beam was 3810 mm and 3581 mm respectively. Same as the modeling method described in Gilton and Uang [11], weld access holes and bolt-related assembly were not considered in the FEM.

### *2.3. 3-D finite element model of RBS-3*

The specimen RBS-3 consisted of one 1400 mm height HW 250×250×9×14 column with one 1500 mm long HN 300×150×6.5×9 beam attached to the weak-axis of column, both of Grade Q235B steel. 3-D finite element model of RBS-3 and grid partition was shown in Fig. 3b. The boundary conditions adopted were the x, y, and z directional displacement restrictions at the column base and the x, y directional displacement restrictions at the column tip followed closely those used in the tests. Axial compression of 786 kN, corresponding to 0.4 times of axial compression ratio, was applied at the top of the column during the test. Weld access holes and bolt-related assembly were considered in this model. Contact between the beam web, shear plate and bolts was explicitly modeled on the basis of the normal and tangential contact property: the normal contact in the contacting surfaces was chosen as “hard”; the tangential contact in the contacting surfaces was defined by penalty function with the frictional coefficient of 0.3.

### *2.4. Verification of the created models*

The experimental results of specimen CW-1 and specimen RBS-3 were used as references to verify the effectiveness of the numerical model through comparing the failure mode, and the load versus displacement hysteretic curves of the test and FEM, as depicted in Figs. 4 and 5 respectively.

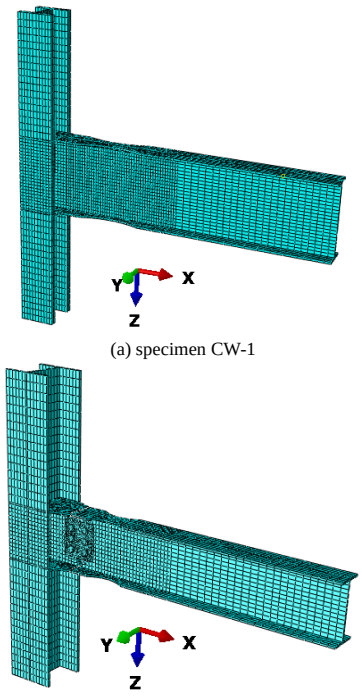


(a) specimen CW-1

(b) specimen RBS-3

**Fig. 3** 3-D finite element model

As seen in Fig. 4, reasonable correlation between the test and FEM was observed, especially in the elastic part that the divergences of the initial stiffness are negligible. The inelastic response of the connection in FEM shows the same trend as test results. Unexpectedly, one can observe from Fig. 4a that the modelling results for specimen CW-1 was basically lower than that of the test, similar with the modelling results conducted by Gilton and Uang [11]. The reason may be that the boundary conditions (through connection plates) in the test were not exactly hinged, resulting in a certain constraint to the rotation of beam and column ends, while the hinge constraint in the FEM was idealized.

As illustrated in Fig. 4b, the numerical curves for specimen RBS-3 were was slightly higher than that of the test, and also smoother and plumper than the experimental curves, which was common and principally caused by ignoring the material damage.

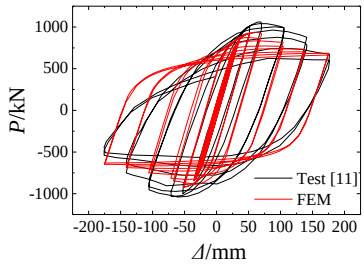


(a) specimen CW-1

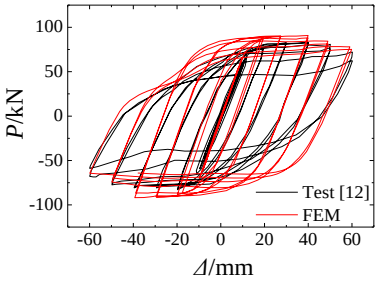


(b) specimen RBS-3

**Fig. 4** Force-displacement hysteretic loops comparison

As evidenced from Figs. 5 and 6, the failure modes of specimen CW-1 and RBS-3 in FEM both demonstrated good correlation with the test results. For specimen CW-1, notably, extensive yielding could be observed in the RBS region. For specimen RBS-3, severe local buckling took place in the portion of weld access holes, indicating that the specimen RBS-3 did not realize the expected target of moving the plastic hinge away from the beam-column connection, and thus leading to the weld fracture in the experimental study.

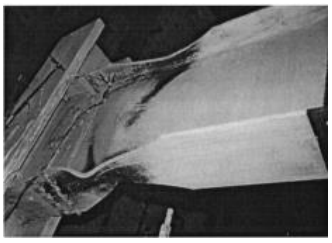

(a) test [11]

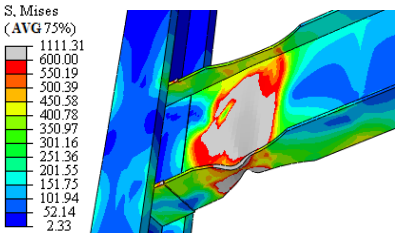


(b) FEM

**Fig. 5** Failure mode comparison of specimen CW-1

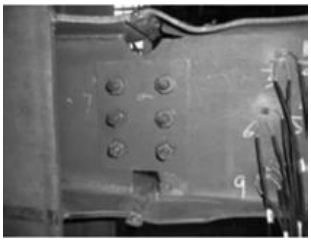

(a) test [12]

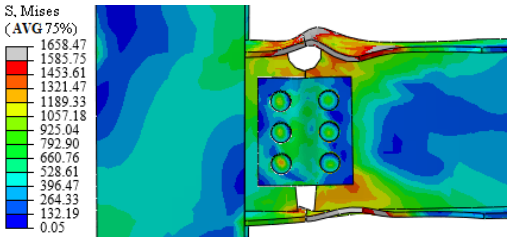


(b) FEM

**Fig. 6** Failure mode comparison of specimen RBS-3

A reasonable agreement between the results of FEM and test for weak-axis connections was generally achieved. Based on this satisfactory correlation study, the modeling methods of specimen RBS-3 was then used to conduct the parametric analysis.

## 3. Comparative analysis of the traditional and developed weak-axis connection

A comparison analysis of the traditional and developed weak-axis connection using numerical methods was performed to discuss the effectiveness of the proposed weak-axis connection. The base model represented an exterior beam-column weak-axis connection in typical moment-resisting frame, which was isolated from the moment inflection points close to the mid-height of the column and mid-span of the beam respectively. Building structure design software PKPM was used to create the steel frame prototype, including four floors with 3000 mm story height, three spans with 4500 mm beam span. The considered load was 6 kN/m$^2$ for dead load and 2 kN/m$^2$ for live load respectively, and thus the internal forces of the structure can be obtained. The substructure was the exterior beam-to-column weak-axis connection prototype in the three floor, and consisted of one 3000 mm height HW 250×250×9×14 column with one 2250 mm long HN 300×150×6.5×9 beam connected through welded-flange and bolted-web connection method, a most widely used connection in Chinese practice engineering.

### *3.1. 3-D finite element model of the traditional connection and developed connection*

The steel grade of column and beam was Q235B, same as the specimen RBS-3, and thus the material properties of the steel profiles in the parametric analysis were the same as those in the validated model RBS-3, described as tri-linear constitutive model, as shown in Fig. 7, with 2.06×10$^5$ MPa elastic modulus. Welds were not considered in FEM as the strength of welds is higher than that of steel plates found in our previous experimental study [17]. The actual beam flange welds are usually defective, and thus the welds material properties were simplified to be the same as steel for the sake of timesaving. Tri-linear constitutive model was also adopted for the material properties of bolts. Table 1 lists the specific values of the material properties. Other modeling methods were the same as described above. Fig. 8 illustrates the traditional weak-axis connection and the developed weak-axis connection in this paper. And the dimensions for two connections were chose to make the end of the connection at basically the same location to make an equivalent comparison.

In order to reflect the actual loading situations, three loading steps were applied in FEM. First, the bolts pretension force was applied through the “bolt load” option in FEM. Second, column axial load of 412 kN, extracted from the PKPM software, was applied to the top of the column. Third, beam tip cyclic loading was applied, as depicted in Fig. 9, whereby the vertical displacement was expressed in the way of the story drift angle, calculated by dividing the beam tip vertical displacement by the length from the beam tip to the column centerline.

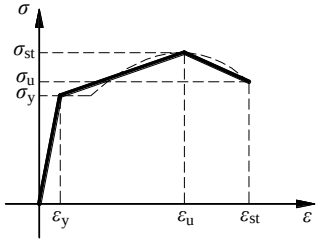


**Fig. 7** Tri-linear constitutive model

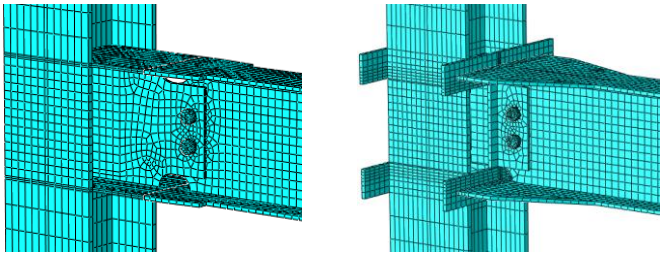

(a) traditional connection (b) developed connection

**Fig. 8** Mesh partition of connection region

**Table 1**
Material properties

| Material | Yield stress $\sigma_y$/MPa | Yield strain $\varepsilon_y$/% | Ultimate stress $\sigma_u$/MPa | Ultimate strain $\varepsilon_u$/% | Failure stress $\sigma_{st}$/MPa | Failure strain $\varepsilon_{st}$/% |
|---|---|---|---|---|---|---|
| Steel | 298.8 | 0.045 | 435.7 | 19.8 | 370.3 | 34.0 |
| Bolt | 940 | 0.024 | 1130 | 9.54 | 960 | 12.54 |

### *3.2. Results comparison of the traditional connection and developed connection*

The force–displacement hysteretic response comparison of the traditional weak-axis connection (TWAC) and developed weak-axis connection (DWAC) under cyclic loading was recorded in Fig. 10. As illustrated in Fig. 10, both the strength and the initial stiffness, determined by the inclination at the elastic stage, of the connection DWAC were slightly greater than those of the connection TWAC. The hysteretic curves of the two connections were stable and repetitive, and the gradual strength degradation was because of the beam buckling. One of the important indexes in evaluation of the seismic performance of beam-column moment connections is its energy dissipation capacity, and it could be measured through the area enclosed by the hysteretic curves. It is obvious that the connection DWAC dissipated more energy than the connection TWAC.

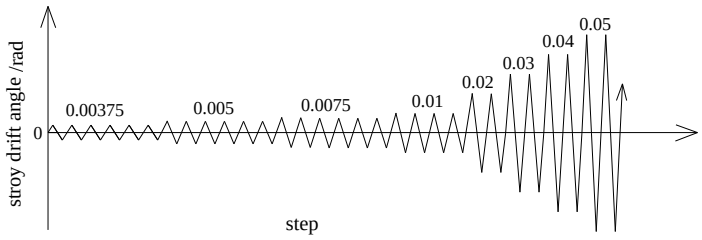


**Fig. 9** Loading protocol

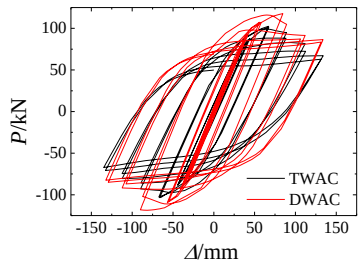


**Fig. 10** Hysteretic loops comparison of specimens TWAC and DWAC

According to the requirement of AISC Seismic Provisions [18], beam-column connections of special moment frame shall be capable of accommodating a story drift angle of at least 0.04 rad. And thus 0.04 rad story drift angle was chosen to elucidate the weak-axis connections response. Figs. 11 and 12 illustrate the Mises stress distribution and equivalent plastic strain (PEEQ) distribution comparison respectively. The stress distribution, strain demand in the beam flange welds indicated the likelihood of potential brittle fracture of the connection. Concentrated stresses and strains were noticed in the weld access holes region for connection TWAC, where the weld fractured in the experimental study [12]. While concentrated stresses and strains were noticed in the beam section at the tips of the widened flange plates for connection DWAC, indicating that the proposed connection details could move the plastic hinge away from the beam-column connection region, and thus protect the beam flange butt welds, and achieve a more reliable structural characteristics.

In summary, comparison results demonstrated that the developed connection details could improve the stiffness, bearing capacity, and energy dissipation ability of weak-axis connection, and also mitigate the stress concentration in the beam flange welds, thus diminishing the possibility of brittle fracture of beam flange welds.

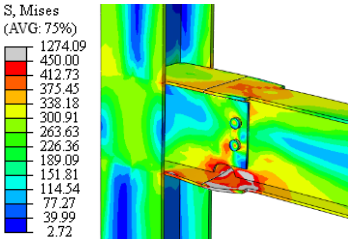


(a) connection TWAC

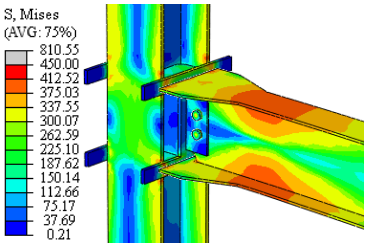


(b) connection DWAC

**Fig. 11** Mises stresses distribution comparison of connections TWAC and DWAC

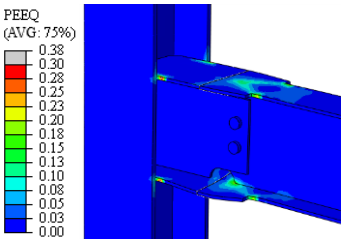


(a) connection TWAC

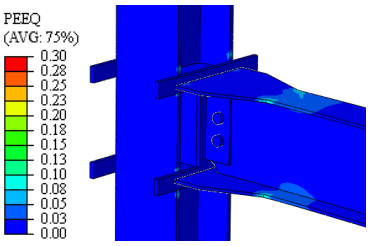


(b) connection DWAC

**Fig. 12** Equivalent plastic strain distribution comparison of connections TWAC and DWAC

### *3.3. Classification of beam-column weak-axis connections based on stiffness*

According to the regulations of Eurocode 3 [19], the steel frame beam-column joints can be classified by stiffness into three categories: rigid, semi-rigid and nominally pinned, as shown in Fig. 13. The abscissa $\theta$ denotes the rotation of a joint, and the ordinate $M$ denotes the moment of a joint at the center of a column. The joint rotation $\theta$ could be obtained through deducting the rotation of a column from the relative rotation of the top and bottom flange of the beam at the joint region [20]. Fig. 14 compares the $M$-$\theta$ hysteretic curves of specimens TWAC and DWAC. As evidenced in Fig. 14, the initial rotational stiffness $S_{j,ini}$ of specimen DWAC was superior to the specimen TWAC, and was 35620 and 33768 kN·m/rad respectively. It is cleared that the

area of the *M*-*θ* hysteretic loops of specimen TWAC was much larger than that of specimen DWAC, indicating that the specimen TWAC dissipated more energy through the joint rotation. This is attributed to that the specimen DWAC has stronger joint region than specimen TWAC, and the specimen DWAC mainly dissipated energy through the plastic hinge rotation on the beam section.

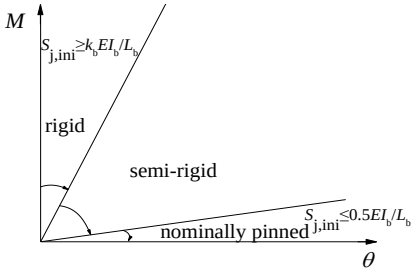


**Fig. 13** Classification of beam-column joints by stiffness

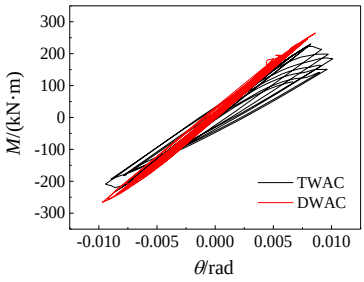


**Fig. 14** *M*-*θ* hysteretic curves comparison

When the initial rotational stiffness $S_{j,ini}$ is larger than $k_b EI_b/L_b$, joints can be classified as rigid, where $E$ represents the elastic modulus, $I_b$ represents the second moment of area of a beam, $L_b$ represents the span of a beam. And the parameter $k_b$ is 8 for frames where the bracing system reduces the horizontal displacement by at least 80%, and 25 for other frames. This reflects that the requirement for rigid joints in weak-support or unsupported frame is stricter. Through comparing the results to the formula in Fig. 13, this two weak-axis connections can be classified as rigid in a strong-bracing system, and be classified as semi-rigid in weak-supported or unsupported system.

## 4. Parametric analysis of the developed weak-axis connection

In order to gain more insight into the mechanical behavior of the proposed weak-axis connection, the influence of geometrical variables of the I-shaped steel plate, widened flange plate on the cyclic behavior was analyzed, and different emphases are adopted for each series. Fig. 15 depicted the dimension parameters of *a*, *b*, *c*, *t*, *d*, and *e*, and Table 2 summarizes the model number and parameter values. For the series A, the variable *a* was the distance between the column flange edge and the I-shaped steel plate edge, and obviously the dimension $2a+h_c$ corresponds to the width of the I-shaped steel plate. For the series B, the variable *b* was the height of flange plate of the I-shaped steel plate. For the series C, the variable *c* was the width of web plate of the I-shaped steel plate. For the convenience of welding between the vertical stiffener and the column web, the variable *c* should not be too wide. For the series T, the variable *t* was the thickness of the I-shaped steel plate. For the series D, the variable *d* was the width of the widened flange plate. For the series E, the variable *e* was the length of the short side of the widened flange plate. In order to realize the smooth transition of the seam section, the ratio of the right side was 1:2.5 based on the Code for seismic design of buildings (GB 50011-2010) [21], thus reducing the stress concentration. As described above, the thickness of widened flange plate was the same as the beam flange. The created models in the parametric analysis changed one parameter at a time while the other conditions are kept the same for the sake of comparison.

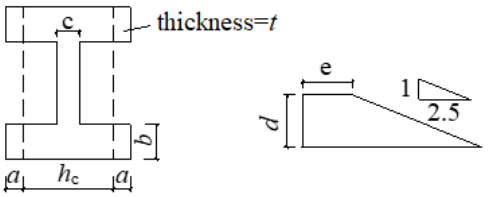


(a) I-shaped steel plate (b) widened flange plate

**Fig. 15** Dimension parameters in the developed weak-axis connection

**Table 2**
Model number and parameter values

| Model | *a*/mm | *b*/mm | *c*/mm | *t*/mm | *d*/mm | *e*/mm |
|---|---|---|---|---|---|---|
| A50 | 50 | 50 | 75 | 14 | 100 | 100 |
| A75 | 75 | 50 | 75 | 14 | 100 | 100 |
| A100 | 100 | 50 | 75 | 14 | 100 | 100 |
| B50 | 100 | 50 | 75 | 14 | 100 | 100 |
| B75 | 100 | 75 | 75 | 14 | 100 | 100 |
| B100 | 100 | 100 | 75 | 14 | 100 | 100 |
| C50 | 100 | 75 | 50 | 14 | 100 | 100 |
| C75 | 100 | 75 | 75 | 14 | 100 | 100 |
| C100 | 100 | 75 | 100 | 14 | 100 | 100 |
| T10 | 100 | 75 | 75 | 10 | 100 | 100 |
| T12 | 100 | 75 | 75 | 12 | 100 | 100 |
| T14 | 100 | 75 | 75 | 14 | 100 | 100 |
| T16 | 100 | 75 | 75 | 16 | 100 | 100 |
| T18 | 100 | 75 | 75 | 18 | 100 | 100 |
| D50 | 100 | 75 | 75 | 14 | 50 | 100 |
| D75 | 100 | 75 | 75 | 14 | 75 | 100 |
| D100 | 100 | 75 | 50 | 14 | 100 | 100 |
| E50 | 100 | 75 | 75 | 14 | 100 | 50 |
| E75 | 100 | 75 | 75 | 14 | 100 | 75 |
| E100 | 100 | 75 | 75 | 14 | 100 | 100 |

To evaluate the local stress concentration, strain demand, as well as the potential for welds cracking, the hysteretic response of the developed weak-axis connection is presented in terms of the Mises index (MI), triaxiality index (TI) and rupture index (RI), which have been used by other researchers [22-23], to reflect the equivalent stress, the triaxial state of stress, and the possibility of fracture at beam flange welds respectively. Based on the report of El-Tawil et al. [22], the fracture strain of the steel material decreases when the value of TI is between -0.75 and -1.5, and the steel material is prone to brittle fracture when the value of TI is less than -1.5. It is more vulnerable to fracture at the beam bottom flange when the flange welds were pulled, and thus the MI, TI and RI distributions at the beam bottom flange welds at the story drift angle -0.04 rad were selected.

### *4.1. Influence of parameters a and b*

Figs. 16 and 17 plots the hysteretic loops of the beam tip load versus beam tip displacement relationship to elucidate the cyclic behavior of series A and B connections respectively. It is observed from Figs. 16 and 17 that the curves almost coincided with each other, indicating that the parameter *a* and *b* slightly affect the connection behavior. And the plastic hinge could all develop in the beam section at the tips of the widened flange plates.

Then the MI, TI and RI distributions at the beam bottom flange welds were compared as recorded in Figs.18 and 19 for series A and B connections respectively. As evidenced from Figs.18 and 19, the maximum value of MI, TI and RI indexes was not at the tips of beam flange welds, which was not consistent with the distribution showed in Fig. 1b, and thus moving the highest stresses away from the start-stop points of a weld, and reducing the potential of the fracture of beam flange welds. This is attributed to the fact that the widened flange plates are able to extend out of the column flanges in the developed weak-axis connection. In comparing these connections, there were

no dramatic differences in MI, TI and RI distributions. The maximum value of MI was less than 1.3, indicating no obvious stress concentration at beam flange welds. The distributions of MI, TI and RI were not completely symmetric, which was due to the bucking deformation of beam flanges.

It can be observed from Fig. 18 that the minimum value of TI was not less than -0.8, indicating that it is less likely to trigger brittle fracture. While Fig. 19 shows clearly that as the parameter *b* increased, the TI and RI values decreased. Lower TI value could cause the reduction in the steel material rupture strain, while larger RI value could increase the potential of weld fracture. That is, too large or too small value for parameter *b* has its negative effects. And too large value for parameter *b* is unfavorable for welding the I-shaped plates to the H-section column. Parameter *b* =75 mm, corresponding to $b_f/2$, was recommended, where $b_f$ represents the width of the beam flange.

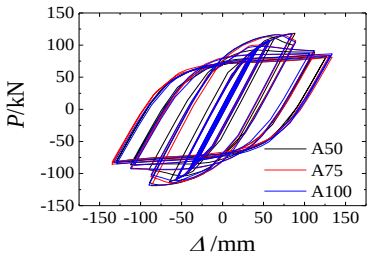


**Fig. 16** Hysteretic loops of series A connections

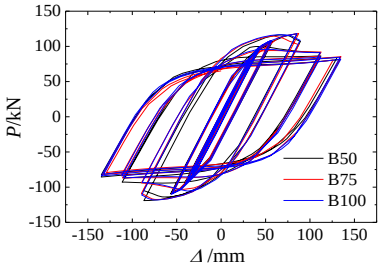


**Fig. 17** Hysteretic loops of series B connections

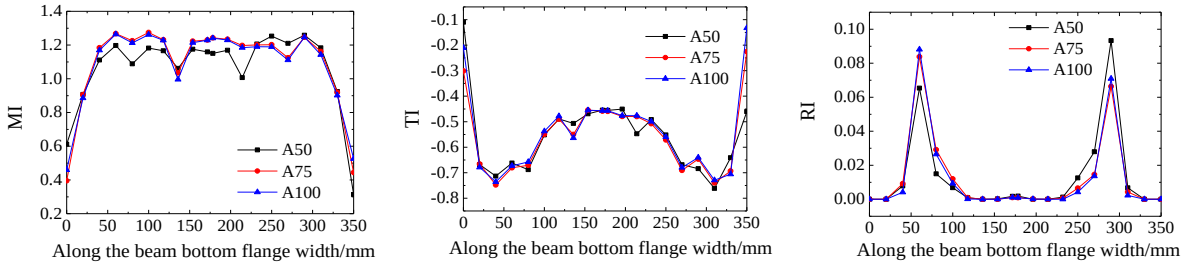


(a) MI distribution (b) TI distribution (c) RI distribution

**Fig. 18** Three indexes distribution of beam bottom flange weld for series A connections

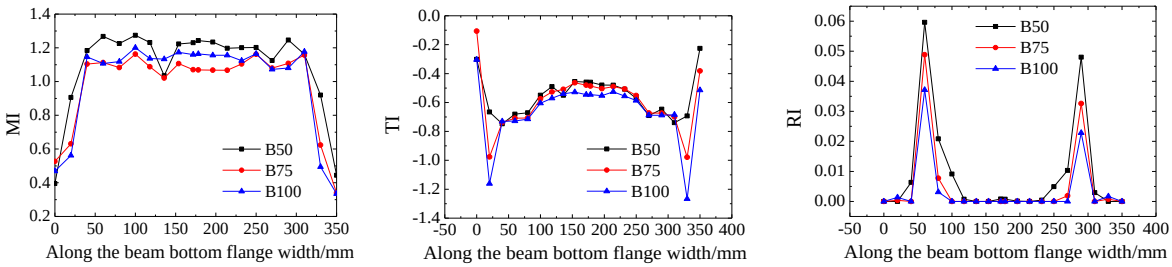


(a) MI distribution (b) TI distribution (c) RI distribution

**Fig. 19** Three indexes distribution of beam bottom flange weld for series B connections

As presented by the FEM, the hysteretic loops, MI, TI, and RI distributions are not very sensitive to the changes in parameter *a*, thus it is only necessary to extend the I-shaped connection plate out of the column flange surface a certain distance. The value of parameter *a* could be adjusted according to the parameter *d*.

### *4.2. Influence of parameter c and t*

Figs. 20 and 21 show the hysteretic loops recorded at the beam end for series C and T connections respectively, As the increase of parameter *c* and *t*, the bearing capacity increased slightly.

Fig. 22 compares the MI, TI and RI distribution at the beam bottom flange welds for series C connections. The MI is basically minimal for specimen C75, and little deviation was observed in the TI and RI distributions. The values of MI, TI and RI are acceptable for the weak-axis connection due to highest plastic equivalent strain appeared a certain distance away from the beam-column interface (see Fig. 12b).

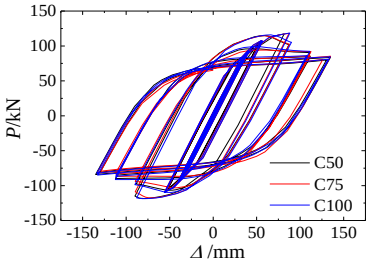


**Fig. 20** Hysteretic loops of series C connections

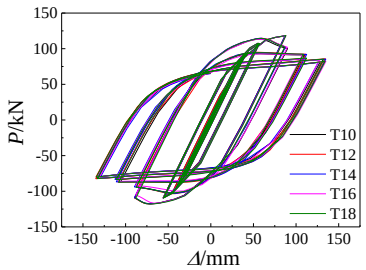


**Fig. 21** Hysteretic loops of series T connections

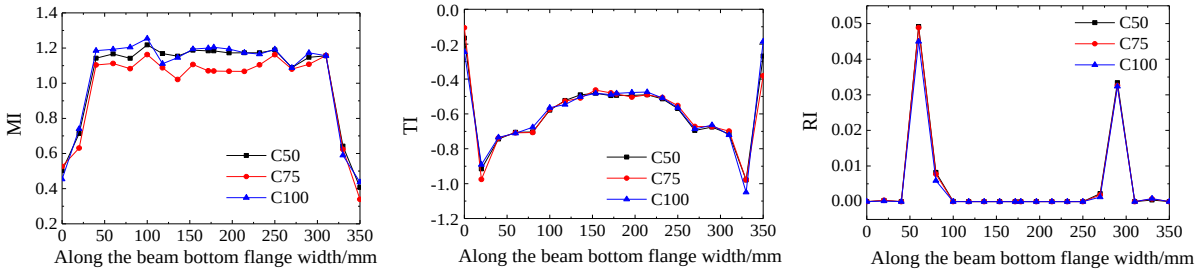


(a) MI distribution (b) TI distribution (c) RI distribution

**Fig. 22** Three indexes distribution of beam bottom flange weld for series C connections

Fig. 23 depicts the$\sigma_{Mises}$, Mises stress, and$\sigma_{S11}$, X-axial stress, which is the stress along the thickness of the I-shaped steel plate, distribution at beam flange welds for series T connections. As we can see,$\sigma_{Mises}$ and$\sigma_{S11}$ distribution of the I-shaped steel plate was consistent for the location at the beam top and bottom flange welds. At the column flange edges, there was the maximum$\sigma_{Mises}$ and$\sigma_{S11}$ stresses, consistent with the Fig. 1b. As the widened flange plate could extend out of the column flanges in the novel weak-axis connection from, the weld edge had minor$\sigma_{Mises}$ and$\sigma_{S11}$ stresses, which was beneficial to reduce the fracture potential of the beam flange welds. As evidenced from Fig. 23, the maximum stress along the thickness of the I-plate$\sigma_{S11}$ was more than 200 MPa, thus the anti-lamellar tearing steel plate was recommended for the I-plate to prevent lamellar tearing which was occurred in our previous experimental study [17]. The stresses of$\sigma_{Mises}$ and$\sigma_{S11}$ are almost the same at the centerline of the I-plate width, indicating that there was only the X-axial stress along the thickness of the I-plate and the stresses in the other two directions are negligible. The trend suggests that the thicker the I-plate, the smaller the maximum stresses at the beam flange groove welds. Hence, the parameter *t* can be taken as slightly greater than the thickness of the column flange.

### *4.3. Influence of parameter d and e*

Figs. 24 and 25 show the hysteretic curves of series D and E connections respectively. Fig. 24 indicates that a larger parameter *d* can increase the initial stiffness and also the bearing capacity. Fig. 25 demonstrates that as parameter *e* increased, the bearing capacity increased slightly.

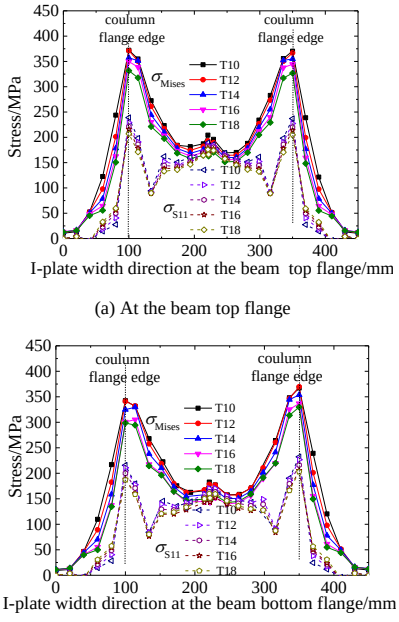


(a) At the beam top flange

(b) At the beam bottom flange

**Fig. 23** Mises stress and X-axial stress distribution of I-plate at beam flange welds for series T connections

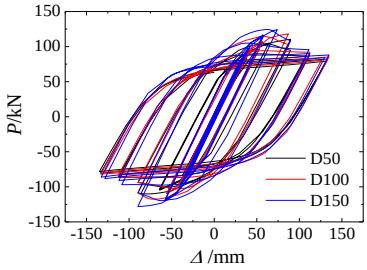


**Fig. 24** Hysteretic loops of series D connections

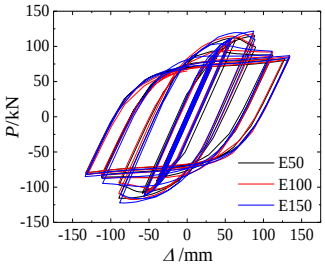


**Fig. 25** Hysteretic loops of series E connections

The MI, TI and RI distribution comparison at beam bottom flange welds for series D connections is included in Fig. 26. It can be seen that the variation of parameter *d* has significant effect on the local stress and strain demand. With the increase of parameter *d*, the length of beam flange welds increases. Due to the aligned edge of widened flange plate and column flange, the most dangerous was at the tips of flange welds for connection D50, similar to Fig. 1b. For connection D100 and D150, the widened flange plate extended 50 and 100 mm respectively out of the column flange, the connection can move the highest stresses away from the start-stop points of a weld. On the other hand, excessive extension of the widened flange plate could not further reduce the stress and strain concentration in the beam flange welds. And thus the widened flange plate extended 50 mm out of the column flange was recommended in the developed weak-axis connection.

Fig. 27 depicts the MI, TI and RI distributions at beam bottom flange welds for series E connections. These figures demonstrate that different values of *e* had relatively small influence on the MI, TI and RI distributions.

Equivalent plastic strain distribution comparison of series E connections and traditional weak-axis connection (TWAC) at the end of 0.06 rad story drift angle loading is summarized in Fig. 28. As observed that extensive local buckling took place in the beam flanges and web at the tips of the widened flange plates for series E connections, indicating the plastic hinge shifted away from the beam-column interface, while the plastic hinge connection TWAC formed at the region of weld access holes, which was more vulnerable to fracture. As the parameter *e* increased, the plastic hinge was further away from the beam-column interface. Based on numerical results, the value of parameter *e* can be set to 100 mm.

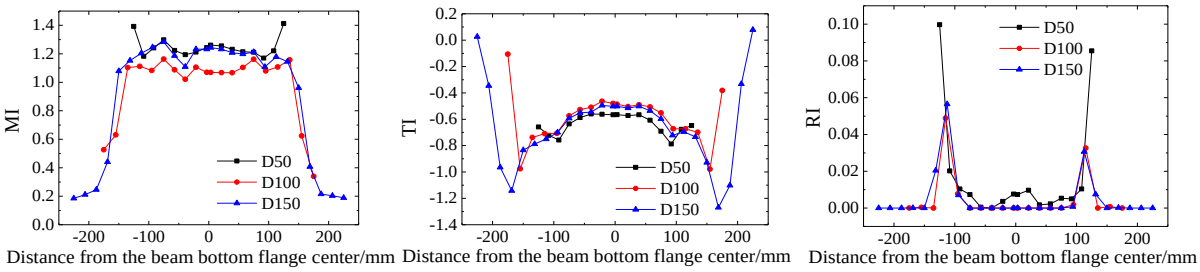


(a) MI distribution (b) TI distribution (c) RI distribution

**Fig. 26** Three indexes distribution of beam bottom flange weld for series D connections

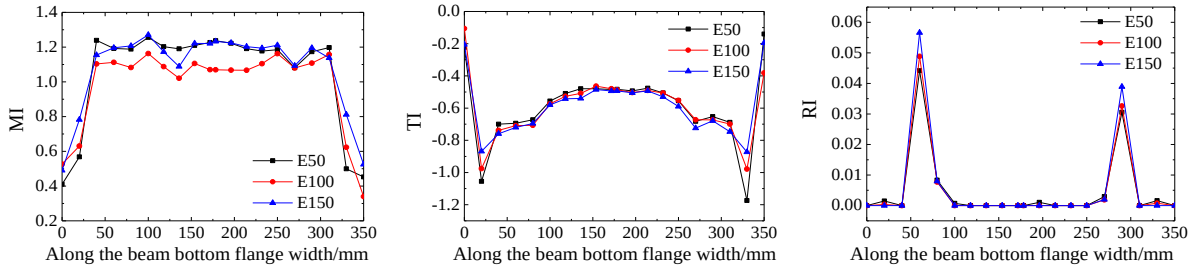


(a) MI distribution (b) TI distribution (c) RI distribution

**Fig. 27** Three indexes distribution of beam bottom flange weld for series E connections

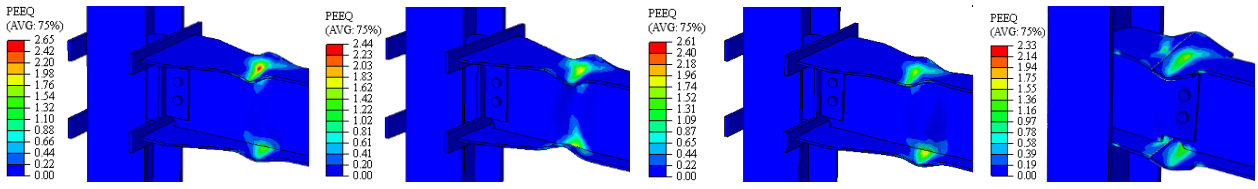


(a) connection E50 (b) connection E100 (c) connection E150 (d) connection TWAC

**Fig. 28** Equivalent plastic strain distribution comparison of series E connections and traditional connection

A parametric analysis was conducted to investigate the influence of I-shaped steel plate and widened flange plate dimension variables on the developed weak-axis connection behavior. From the above discussion, it is suggested that the value of parameters $b$ and $c$ can be set to 75 mm (about $b_f/2$). And the value of parameters $d$ and $e$=100 mm is reasonable for use in the adopted connection details and sizes of beam and column. That is, it is judged that extending the widened flange plate 50 mm out of the column flange is enough to move the highest stresses away from the start-stop points of a weld and thus avoiding brittle failure of the beam bottom flange groove welds. The widened flange plate extended 50 mm out of the column flange was recommended, and thus the parameter $a$ can be set to 50 mm or slightly larger. The parameter $t$ can be taken as slightly greater than the thickness of the column flange.

## 5. Design procedures of the developed weak-axis connections

### *5.1. Design procedures*

Based on the results of FEM, design procedures for the developed weak-axis moment connections was proposed.

First, for designed steel beam and column section, the horizontal stiffeners and vertical stiffeners of I-shaped plates (see Fig. 2b) can be determined with the thickness slightly greater than the beam flange and beam web respectively.

Second, the anti-lamellar tearing steel plate can be used for the I-shaped steel plate with the thickness slightly greater than the thickness of the column flange. The distance between the column flange edge and the I-shaped steel plate edge $a$ can be set to 50 mm or slightly larger, and thus the width of the I-shaped steel plate can be set to $h_c$+2$a$, where $h_c$ represents the height of the column section. The height of flange plate of the I-shaped steel plate $b$, and the width of web plate of the I-shaped steel plate $c$ can be set to $b_f/2$, where $b_f$ represents the width of the beam flange.

Then, it is reasonable to extend the widened flange plate 50 mm out of the column flange for design purposes, and thus the width $d$ of the widened flange plate can be set to [($h_c$-$b_f$)/2+50] mm. The length $e$ of the short side of the widened flange plate can be set to 100 mm, and then the ratio of the right side can be set to 1:2.5 to realize the smooth transition of the beam section. And thus the length of the long side of the widened flange plate is $e$+2.5[($h_c$-$b_f$)/2+50].

To ensure that the designed weak-axis connections can meet the seismic design requirement of “strong joint and weak member”, and move the plastic hinge away from the beam-column interface, the following checking calculation need to be conducted.

1) Determine the maximum plastic moment $M_{pr}$ of steel beam at the location of the expected plastic hinge:

$$M_{pr} = C_{pr} Z_b R_y F_y \tag{1}$$

Where, $C_{pr}$ is the enhancement coefficient considering strain strengthening, local constraints, etc, and can be set to 1.15 for China’s steel products [24]; $Z_b$ represents the plastic section modulus of the beam section; $R_y$ is a multiplier accounting for expected material overstrength, and can be set to 1.1 for China’s steel products [24]; $F_y$ represents the nominal yield strength.

2) Calculate the moment demand at the beam-column interface according to the bending moment distribution gradient on the beam:

$$M_{dem\,j} = \frac{L_b}{L_b - L_p} M_{pr} \tag{2}$$

Where, $L_b$ and $L_p$ is the distance from the beam span center to the beam end and the distance from the plastic hinge center to the beam end. And the $L_p$ can be set to the length of the widened flange plate plus 1/4 $h_b$ [110], where $h_b$ represents the height of the beam section.

3) Determine the design flexural capacity $M_{cap,j}$ at the beam-to-column

interface:

$$M_{\text{cap, j}} = \alpha M_{\text{dem, j}} \tag{3}$$

Where, parameter α is a multiplier and can be set to 1.1 based on the recommendation of Chen et al. [25].

4) Check the beam end reinforcement section based on the design flexural capacity $M_{\text{cap,j}}$:

$$M_{\text{cap,j}} \le C_{\text{pr}} Z_{\text{b}}' R_{\text{y}} F_{\text{y}} \tag{4}$$

Where, $Z_{\text{b}}'$ represents the plastic section modulus of the steel beam section and the widened flange plates section at the beam-to-column interface.

If the results doesn't meet the formula (4), the parameters of the widened flange plates need to be further adjusted. Meanwhile, as the widened flange plates are adopted, it is necessary to check the requirement of "strong column and weak beam" based on GB 50011-2010 [21].

### *5.2. Numerical example*

To verify the applicability of the proposed dimensions to other beam and column sections, a developed beam-column weak-axis connections DWAC-2 with different beam-column sections were modelled and analyzed through FEM. The beam section HN 350×175×7×11and column section HW 300×300×10×12 were taken from test specimens in our previous study [26]. Based on the results of FEM, the parameter $a$=50 mm, $b$=$c$=$b_{\text{f}}$/2, $d$=($h_{\text{c}}$-$b_{\text{f}}$)/2+50, and $e$=100 mm was adopted for connection DWAC-2. The modeling methods and loading system were exactly the same as described above.

Fig.29 shows the load-displacement hysteretic curves and also the Equivalent plastic strain (PEEQ) distribution of the joint region at the story drift angle of 0.04 rad. We can observe that the load-displacement hysteretic curves of connection DWAC-2 were stable and repetitive, and the gradual strength degradation was due to the beam buckling at the end of widened flange plates. Plastic strain was basically concentrated at the beam section away from the beam-column interface, indicating that the recommended dimensions of I-shaped plates were also applicable to DWAC-2 with different beam-column sections.

## 6. Conclusions

In this paper, a parametric study was conducted to verify the cyclic behavior of the proposed weak-axis connections using an innovative solution to enhance the beam-column connection. The following conclusions can be drawn on the basis of the finite element analysis results.

1) A good correlation between the test and FEM is obtained.

2) The proposed weak-axis connections could move the highest stresses away from the start-stop points of a weld, and then shift the plastic hinge away from the beam-column interface to prevent premature brittle flange weld failure, while the local buckling occurred in the weld access holes region in the traditional weak-axis connection.

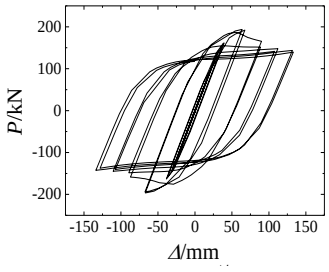


(a) Load-displacement hysteretic curves

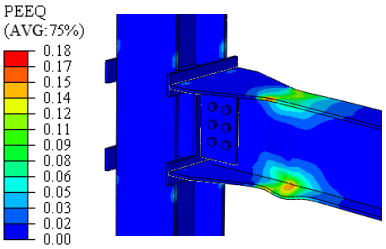


(b) Equivalent plastic strain distribution

**Fig. 29** Hysteresis performance of connection DWAC-2

3) The developed weak-axis connections can be classified as rigid in a strong-bracing system, and be classified as semi-rigid in weak-supported or unsupported system.

4) As there is greater stress in the thickness direction of the I-shaped steel plate, the anti-lamellar tearing steel plate is recommended for the I-shaped steel plate. The parameter $t$ can be taken as slightly greater than the thickness of the column flange.

5) The hysteretic loops, the MI, TI and RI distributions are not very sensitive to the changes of parameter $a$, $b$, $c$, and $e$. It is suggested that the value of parameters $b$, $c$ and $e$ can be set to $b_{\text{f}}$/2, $b_{\text{f}}$/2 and 100 mm respectively, where $b_{\text{f}}$ represents the width of the beam flange. With the increase of parameter $d$, the greater the bearing capacity of connections, and also the greater the distance between the start-stop points of welds and the peek stresses, which could reduce the premature brittle failure of flange welds. Extending the widened flange plate 50 mm out of the column flange is recommended in the developed weak-axis connection, and thus the parameter $a$ can be set to 50 mm or slightly larger.

6) The parametric study presented in this paper provides a first insight into the hysteretic responses of the developed weak-axis connection with I-shaped plates. More experimental investigation is required to fully assess this behavior.

## Acknowledgements

The authors would like to thank the financial support provided by Basic Research Plan Project of Natural Science of Shaanxi Province (2019JQ-272) and the Special Scientific Research Plan Project of Education Department of Shaanxi (19JK0481) for the financial support.

## References

[1] T. Kim, A.S. Whittaker, A.S.J. Gilani, et al., Cover-plate and flange-plate steel moment-resisting connections, J. Struct. Eng. ASCE 128 (2002) 474-482.
[2] C.H. Lee, J.H. Jung, M.H. Oh, et al., Cyclic seismic testing of steel moment connections reinforced with welded straight haunch, Eng. Struct. 25 (2003) 1743-1753.
[3] C.C. Chen, C.C. Lin, Seismic performance of steel beam-to-column moment connections with tapered beam flanges, Eng. Struct. 48 (2013) 588-601.
[4] X. Chen, G. Shi, Experimental study on seismic behavior of cover-plate joints in high strength steel frames, Eng. Struct. 191 (2019) 292-310.
[5] J. Jin, S. El-Taxil, Seismic performance of steel frames with reduced beam section connections, J. Constr. Steel Res. 61 (2005) 453-471.
[6] S.L. Jones, G.T. Fry, M.D. Engelhardt, Experimental evaluation of cyclically loaded reduced beam section moment connections, J. Struct. Eng. ASCE 128 (2002) 441–451.
[7] D.T. Pachoumis, E.G. Galoussis, C.N. Kalfas, et al., Cyclic performance of steel moment-resisting connections with reduced beam sections-experimental analysis and finite element model simulation, Eng. Struct. 32 (2010) 2683-23102.
[8] S. Momenzadeh, M.T. Kazemi, M.H. Asl, Seismic performance of reduced web section moment connections, Int. J. Steel Struct. 17 (2017) 413-425.
[9] C.S. Gilton, C.M. Uang, Cyclic response and design recommendations of weak-axis reduced beam section moment connections, J. Struct. Eng. ASCE 128 (2002) 452-463.
[10] FEMA-355D State of the art report on connection performance, Federal Emergency Management Agency, Washington, DC, 2000.
[11] B.S. Guo, Hysteretic behavior and design criterion of beam-to-column web connections in steel moment frames under cyclic load, Xi'an University of Architecture & Technology, Xi'an, 2004. (in Chinese)
[12] Y.S. Yu, J. Wang, W.P. Huang, et al., Experimental study on the failure mode of reduced beam section connections of the bolted-welded connection of steel frame beam-column about minor axis, Building Structure, 44 (2014) 30-33. (in Chinese)
[13] K. Oh, K. Lee, L. Chen, et al., Seismic performance evaluation of weak-axis column-tree moment connections with reduced beam section, J. Constr. Steel Res. 105 (2015) 28-38.
[14] S.D. Kim, S.S. Kim, Y.K. Ju, Strength evaluation of beam-column connection in the weak axis of H-shaped column, Eng. Struct. 30 (2008) 1699-1710.
[15] W.L. Li, J.P. Hao, L.K. Wang, et al., Experimental and analytical study on stiffness of beam-to-column minor axis top-and seat angle connection in steel frames, Journal of Building Structures, 29 (2008) 125-131.
[16] Z. Wang, T. Wang, Experimental and finite element analysis for the end plate minor axis connection of semi-rigid steel frames, China Civil Engineering Journal, 45 (2012) 83-89.
[17] L.F. Lu, Y.L. Xu, H. Zheng. Investigation of composite action on seismic performance of weak-axis column bending connections, J. Constr. Steel Res. 129 (2017) 286-300.

[18] ANSI/AISC 341-10 Seismic provisions for structural steel buildings, AISC, Chicago, 2010.
[19] Eurocode 3 Design of steel Structures Part 1-8: Design of joints, London, 2003.
[20] G. Shi, F. Yuan, D. Huo, et al., The theoretical model and measuring calculation method of the beam-to-column joint rotation in steel frame, Engineering Mechanics, 29 (2012) 52-60. (in Chinese)
[21] GB 50011-2010 Code for seismic design of buildings, China Architecture & Building Press, Beijing, 2010. (in Chinese)
[22] S. El-Tawil, T. Mikesell, E. Vidarsson, et al., Strength and ductility of FR welded-bolted connection, SAC Rep. No. 108-01, SAC Joint Venture, Sacramento, Calif, 1998.
[23] F. Hu, G. Shi, B. Yu, et al., Seismic performance of prefabricated steel beam-to-column connections, J. Constr. Steel Res. 102 (2014) 204-216.
[24] Y.Y. Cai, Beam-column connection design of steel frame considering shift away of plastic hinge, Building Structure, 34 (2004) 3-10. (in Chinese)
[25] C.C. Chen, C.A. Lu, C.C. Lin, Parametric study and design of rib-reinforced steel moment connections, Eng. Struct. 27 (2005) 699-708.
[26] L.F. Lu, Y.L. Xu, T.H. Zhou, et al., Experimental research on box strengthened joint connection for weak axis of I-section column-H-shaped beam, Journal of Building Structures, 37 (2016) 73-80.